



Research

Cite this article: Secchi E, Rusconi R, Buzzaccaro S, Salek MM, Smriga S, Piazza R, Stocker R. 2016 Intermittent turbulence in flowing bacterial suspensions. *J. R. Soc. Interface* **13**: 20160175.
<http://dx.doi.org/10.1098/rsif.2016.0175>

Received: 1 March 2016

Accepted: 25 May 2016

Subject Category:

Life Sciences—Physics interface

Subject Areas:

biophysics, environmental science

Keywords:

bacterial turbulence, collective dynamics, microfluidics

Author for correspondence:

Roman Stocker

e-mail: romanstocker@ethz.ch

Electronic supplementary material is available at <http://dx.doi.org/10.1098/rsif.2016.0175> or via <http://rsif.royalsocietypublishing.org>.

Intermittent turbulence in flowing bacterial suspensions

Eleonora Secchi^{1,2}, Roberto Rusconi^{2,3}, Stefano Buzzaccaro¹,
M. Mehdi Salek^{2,3}, Steven Smriga^{2,3}, Roberto Piazza¹ and Roman Stocker^{2,3}

¹Department of Chemistry (CMIC), Politecnico di Milano, via Ponzio 34/3, 20133 Milano, Italy

²Ralph M. Parsons Laboratory, Department of Civil and Environmental Engineering, Massachusetts Institute of Technology, 02139 Cambridge, MA, USA

³Department of Civil, Environmental and Geomatic Engineering, Institute for Environmental Engineering, ETH Zurich, 8092 Zurich, Switzerland

Dense suspensions of motile bacteria, possibly including the human gut microbiome, exhibit collective dynamics akin to those observed in classic, high Reynolds number turbulence with important implications for chemical and biological transport, yet this analogy has remained primarily qualitative. Here, we present experiments in which a dense suspension of *Bacillus subtilis* bacteria was flowed through microchannels and the velocity statistics of the flowing suspension were quantified using a recently developed velocimetry technique coupled with vortex identification methods. Observations revealed a robust intermittency phenomenon, whereby the average velocity profile of the suspension fluctuated between a plug-like flow and a parabolic flow profile. This intermittency is a hallmark of the onset of classic turbulence and Lagrangian tracking revealed that it here originates from the presence of transient vortices in the active, collective motion of the bacteria locally reinforcing the externally imposed flow. These results link together two entirely different manifestations of turbulence and show the potential of the microfluidic approach to mimic the environment characteristic of certain niches of the human microbiome.

1. Introduction

Many species of bacteria live in confined environments, such as animal guts [1], marine detritus [2] and soil [3], where they may attain very high cell densities. In the human gastrointestinal tract, bacteria can reach densities of 10^{10} cells ml^{-1} or more [4] and can affect virulence mechanisms and increase antibiotic resistance through horizontal gene transfer [1]. Understanding the behaviour of dense suspensions of bacteria can provide windows into these difficult-to-observe microbial environments and may offer potential biophysical context for the intense efforts to describe the composition and functions of bacteria in the human microbiome. In recent years, dense suspensions of motile microbes have also represented an intriguing experimental [5–8] and theoretical [9,10] model system in the field of ‘active physics’: they allow one to profitably explore general principles of collective dynamics, because their spatio-temporal scales, organism densities and overall control over experimental conditions are far more tractable than classic model systems of collective dynamics, such as fish schools and bird flocks [11–13].

At high bacterial densities, flow patterns emerge in the suspension that have spatial scales one to two orders of magnitude larger than a single bacterium and are characterized by the presence of continuously morphing eddies and jets that have suggested the analogy with classic turbulent flow of simple fluids at high Reynolds numbers, resulting in the label ‘bacterial turbulence’ [8]. This similarity is surprising in view of the strong difference in the physical mechanisms generating vorticity in ordinary turbulence and in bacterial turbulence and has remained primarily qualitative. Here, we deepen the connection between classic turbulence and bacterial turbulence through novel experiments in which a dense bacterial

suspension is flowed in a microfluidic channel. These experiments on the one side provide a direct analogue with classic turbulence experiments, and on the other side represent a controlled model system for the often flowing, microbially dense human gut. The application of an external flow on a dense bacterial suspension led us to discover an intermittency phenomenon in the suspension at small imposed flow rates, which parallels the intermittency characteristic of the onset of ordinary turbulence [14] and shows that microbially dense environments can be characterized by considerable, system-intrinsic unsteadiness.

2. Material and methods

2.1. Bacterial strains and culture conditions

The bacterial strains used in this work were *Bacillus subtilis* wild-type strain OI1085 (4 μm in length, 1 μm in diameter). Cells were grown on Terrific Broth (TB, [15]) agar plates from a frozen stock solution. A single colony from the plate was used to inoculate a 5 ml TB solution. Cultures were incubated overnight at 30°C while shaking at 150 r.p.m. An aliquot of the overnight culture (1 ml) was inoculated to a fresh batch (50 ml) of prewarmed TB and incubated approx. 5–7 h until the culture reached the stationary phase. Before the experiment, the culture was centrifuged at 5000g for 5 min and the pellet was resuspended in 500 μl of fresh TB by gentle vortexing in order to keep cells intact and motile. To quantify cell densities, an aliquot of the bacterial suspension was amended with 0.2% (final concentration) formaldehyde to kill cells, diluted 1:200 and injected into a 6 μm -high microfluidic channel for cell counting. Four images with an area of 2.3 mm^2 from different parts of the channel were acquired and the number of bacteria contained in each volume was determined. The typical number of cells counted in one image was between 900 and 1400 depending on the initial concentration of the sample (corresponding, respectively, to a final concentration of 1.3×10^{10} cells ml^{-1} and 2×10^{10} cells ml^{-1}) and the standard deviation on the order of 4%.

2.2. Microfluidic experiments

We fabricated polydimethylsiloxane (PDMS) channels using standard soft lithography techniques [16]. PDMS microchannels were plasma-sealed onto a glass slide, on which previously a 300 μm -thick layer of PDMS had been deposited so that all boundaries of the microchannel were made of the same material. The microfluidic channel was connected to the syringes through gas permeable tubes (Silicone Tubing, VWR International) which, in addition to the small lateral dimension of the channel and the permeability of PDMS to gases [17], ensured sufficient oxygen supply to maintain cell motility. Imaging of bacterial suspensions in flow was performed on an inverted microscope (Ti-Eclipse, Nikon, Japan) equipped with a digital camera (either Andor Neo 5.5 sCMOS; 2560×2160 pixels, $6.5 \mu\text{m}$ pixel $^{-1}$; or Photron SA3; 1024×1024 pixels, $17 \mu\text{m}$ pixel $^{-1}$). Images were acquired using bright-field microscopy with a $30\times$ magnification. The frame rate—370 fps with the Andor Neo 5.5 sCMOS and 5000 fps with the Photron SA3 60 K—was chosen based on the magnitude of the imposed flow rate. For the microrheology measurements, images were acquired in bright field at 10 fps (with the Andor Neo 5.5 sCMOS) and $10\times$ magnification.

2.3. Optical measurements of bacterial motion and density

The dense suspension (2×10^{10} cells ml^{-1}) was imaged using a recently developed optical correlation technique, ghost particle

velocimetry (GPV) [18], which yielded the velocity field in the suspension without the need of tracer particles. GPV measurements are based on monitoring the displacement in time of the speckle pattern generated in the image plane by a sample illuminated with a spatially partially coherent light source, such as a microscope condenser with reduced aperture. GPV allows to quantitatively map the fluid velocity field by calculating the time correlation function of the normalized intensity of the light scattered by nanometric size scatterers.

The working optical principles of GPV are the following. The light intensity scattered by N particles can be written as $E_s(q; t) = B(q; t) E_0(t)$, where $E_0(t)$ is the incident field and $B(q; t) = \sum_i b_i(q) \exp[iq \cdot r_i(t)]$ is the total scattering amplitude, in which $b_i(q)$ is the Fourier transform of the refractive index distribution of a single particle. In the so-called heterodyne configuration, the ensemble average of the scattering intensity is equal to zero, but the variance is a finite quantity proportional to the number of particles, N , which is given by

$$\sigma_s^2(q) = N[b(0)]^2 P(q) S(q),$$

where $P(q)$ is a factor that depends on the single particle geometrical properties and $S(q)$ is the form factor which depends on the particles' reciprocal positions. The variance of the image in the Fourier space is then defined as

$$\sigma_s^2(\Delta t) = \int |F_D(q; \Delta t)|^2 dx dy,$$

where $|F_D(q; \Delta t)|^2 = A(q)[1 - \exp(-\Delta t/\tau(q))] + B(q)$ and contains the term $A(q)$, which depends also on the number of scattering centres in the scattering volume. For uncorrelated images,

$$|F_D(q; \Delta t)|^2 = B(q) + A(q) = \sigma_s^2(\Delta t),$$

which contains, through $A(q)$, information on the number of particles within a given scattering volume. As $A(q)$ depends also on the characteristics and the illumination properties of the microscope, the precise measurement of the concentration of the scatterers requires an accurate calibration (see electronic supplementary material, figure S1). In our experiments, the information on the local concentration of the scatterers was obtained by calculating the variance of the image as

$$\sigma^2(x, y) = \left\langle \left(\frac{i_s(x, y; t)}{i_s(t)} - 1 \right)^2 \right\rangle_t,$$

where $i_s(x, y; t)$ is the total intensity detected by the camera and $i_s(t) = \langle i_s(x, y; t) \rangle_{x,y}$ was obtained by averaging in time over 50 successive frames. The local flow velocity is measured from the displacement of the speckle pattern using an adapted microparticle image velocimetry (μPIV) algorithm [19].

2.4. Microrheology measurements

The viscosity of the bacterial suspensions was measured using a microfluidic Y-shaped channel (80 μm deep, 1 mm wide). A detailed description of the method can be found in [20]. Briefly, the technique is based on the determination of the interface position between two fluids of different viscosity, entering the channel side-by-side. The ratio of the viscosities between the two fluids can be determined from the ratio of the widths between the two streams.

2.5. Numerical simulations

A finite-element code (COMSOL Multiphysics, Burlington, MA) was used to perform two-dimensional numerical simulations of an incompressible flow in a channel with the same dimensions as the horizontal projection of the channel used in the experiments (width, $W = 180 \mu\text{m}$; length, $L = 2000 \mu\text{m}$) and the measured dependence of the viscosity η on the mean shear rate S . The width of the channel was extrapolated from the parabolic fit

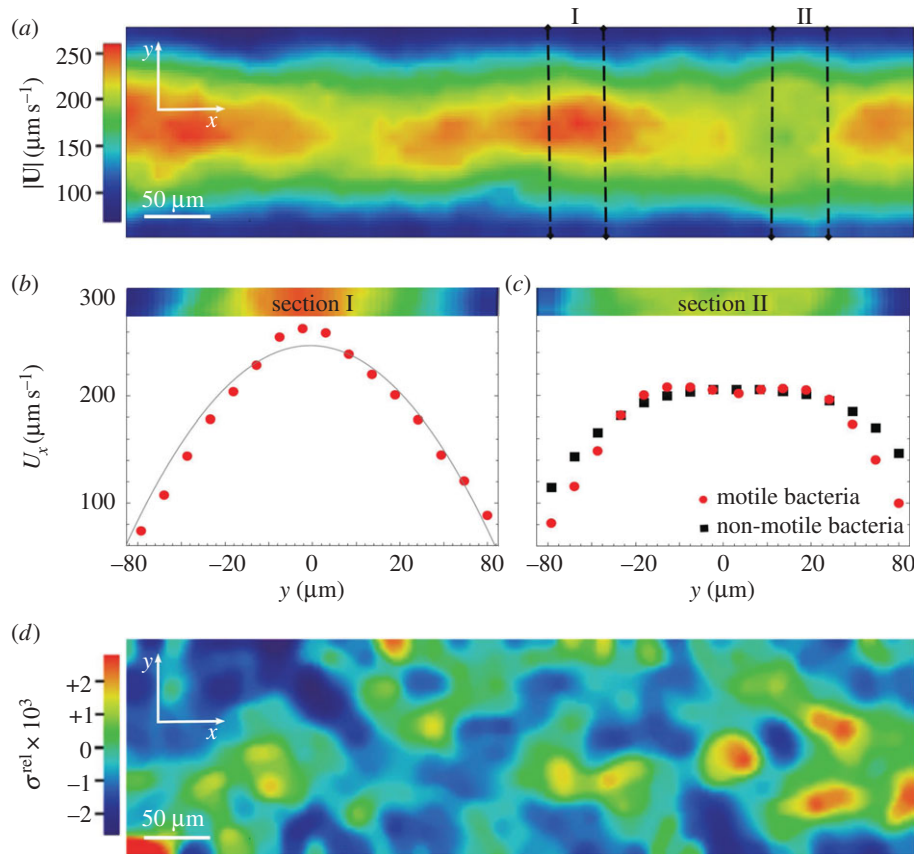


Figure 1. (a) Snapshot of the magnitude of the in-plane velocity, $|\mathbf{U}| = (U_x^2 + U_y^2)^{1/2}$, in a suspension of *Bacillus subtilis* bacteria subject to a flow along the x direction at a mean velocity of $190 \mu\text{m s}^{-1}$ (corresponding to a mean absolute shear rate of $S = 2.2 \text{ s}^{-1}$). The cell concentration was $2 \times 10^{10} \text{ cells ml}^{-1}$, equivalent to a volume fraction of approximately 6.3%. The channel was $320 \mu\text{m}$ deep, $200 \mu\text{m}$ wide and an $840 \mu\text{m}$ long section is shown. The image was obtained by ghost particle velocimetry (GPV) from a video acquired at the channel mid-depth. (b,c) Cross-channel profiles of the streamwise velocity U_x (red circles) corresponding to section I (b) and section II (c) in (a), averaged along x over the width of the sections indicated in (a). Also shown are the velocity profiles for a dilute suspension of small polystyrene spheres (solid line in b) and for a dense suspension of dead (i.e. non-motile) bacteria (black squares in (c)). (d) Concentration fluctuations in the suspension are very small, as demonstrated by the small values of the relative excess standard deviation $\sigma^{\text{rel}}(x, y) = \langle (i_s(x, y; t)/i_s(t) - 1)^2 \rangle_t^{1/2}$ computed from GPV.

of the flow profile obtained with a dilute suspension of 200 nm polystyrene spheres (figure 1b).

2.6. Vortex identification and tracking

We analysed the dynamics of vortices in the flowing bacterial suspensions by employing the so-called λ -2 criterion [21]. According to this criterion, one can find vortex cores as connected regions that have two negative eigenvalues of the symmetric tensor $\Delta^2 + \Omega^2$, where Δ and Ω are, respectively, the symmetric and anti-symmetric portions of the velocity gradient tensor and the latter was computed directly from the velocity field obtained with the GPV technique.

3. Results and discussion

Tracking the flowing dense suspensions, we observed that the velocity field \mathbf{U} displayed strong intermittency along the flow direction, x (figure 1a). The intermittency takes the form of changes in the cross-stream profile of the streamwise velocity, $U_x(y)$ (figure 1b,c; the subscript indicates the velocity component), which alternates between a parabolic profile (figure 1b, red circles) and a plug-flow profile (figure 1c, red circles). A parabolic profile is characteristic of dilute suspensions of colloidal particles in Newtonian fluids and was recovered in our set-up when we flowed a dilute suspension of 200 nm polystyrene

spheres (figure 1b, full line). The flat-top structure of the plug-flow profile is generally the signature of shear-thinning fluids [22] and of concentrated suspensions of rigid rods [23].

The intermittent flow profile originated from the motility of the bacteria. This was shown by control experiments with dense flowing suspensions of dead *B. subtilis* cells, at the same cell concentration, in which the flow field exhibited a continuous plug-flow profile without intermittency (figure 2). The absence of intermittency in flowing suspensions of dead bacteria also allowed us to rule out the eventuality that this phenomenon could stem from potential artefacts related to any unsteadiness in the externally imposed flow. The intermittency in the velocity field was not accompanied by fluctuations in cell concentration (figure 1d), implying that tracking the motion of bacteria, as done by GPV, yielded the velocity field of the suspension as a whole, including the bacteria and the suspending fluid.

Experiments with imposed flows of different magnitude showed that the strongest spatial intermittency occurred for the lowest flow rate applied, which corresponded to a mean velocity of approximately $100 \mu\text{m s}^{-1}$ (figure 3a). This flow velocity is approximately twice the characteristic velocity of bacterial turbulence in the absence of flow (approx. $40 \mu\text{m s}^{-1}$; electronic supplementary material, figure S2), measured for the same bacterial concentration used in the experiments with flow. The intermittency progressively decreased with increasing

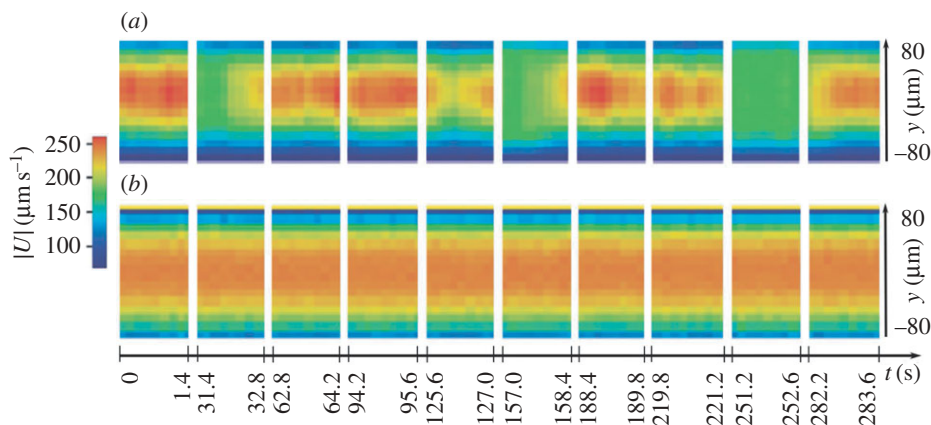


Figure 2. (a) Velocity field in a dense suspension of motile bacteria flowing from left to right at a flow rate $Q = 25 \mu\text{l h}^{-1}$. The cell concentration was 2×10^{10} cells ml^{-1} . The sequence of 10 panels represents a time-lapse view of the velocity profile across the channel (y direction), with one 1.4 s-long recording every 30 s, for a total time of about 285 s. (b) Velocity field in a dense suspension of non-motile bacteria. All other conditions were as in (a).

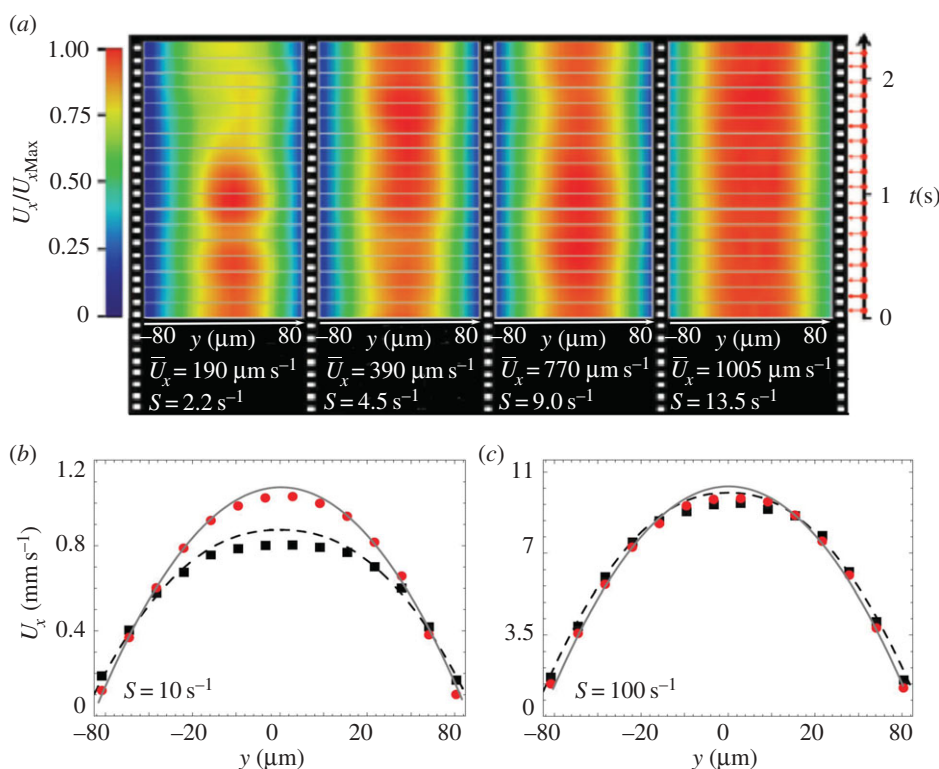


Figure 3. (a) Time-lapse reconstruction of the cross-channel profile of the streamwise velocity U_x at a fixed longitudinal position x , for four values of the flow rate. For each flow rate, the velocity field $U_x(y, t)$ was determined by interpolation from data acquired at a rate of 370 s^{-1} . U_x was normalized by its maximum value ($U_{x\text{Max}}$) calculated in a time interval of 0.14 s. The mean velocity and the mean absolute value of the shear rate, S , across the channel are given for each case. (b,c) Cross-channel profiles of the streamwise velocity, U_x (red circles), for a mean absolute shear rate of $S = 10 \text{ s}^{-1}$ (b) and 100 s^{-1} (c). Also shown are the velocity profiles for a dense suspension of dead (i.e. non-motile) bacteria (black squares) and for a dilute suspension of small polystyrene spheres (solid lines). Results are compared with the numerical solution (dashed lines) of the flow using the dependence of viscosity on mean shear rate obtained from microrheological measurements [20].

flow rate, but completely disappeared only at mean flow velocities exceeding $390 \mu\text{m s}^{-1}$ (see the third and fourth panels in figure 3a), which is approximately 10-fold larger than the characteristic velocity of the bacterial motion. An increase in flow rate also reduced the difference in the flow profiles of motile and non-motile bacteria, which both approached a parabolic flow profile (figure 3b,c). The shear rates used in these experiments (2.2 – 13.5 s^{-1}) are comparable to those that have been measured in the human gut (0.2 – 8 s^{-1} ; [24]).

We hypothesized that the differences in the velocity profiles occurring in the intermittent flow may be caused by local differences in the effective rheology of the suspension, η_{eff} . Through microrheology experiments (see §2.4), we found

that the viscosity of a dense *B. subtilis* suspension, compared to that of their suspending medium, as a function of the mean shear rate displayed two distinct regions (figure 4a). For $S < 3 \text{ s}^{-1}$, the viscosity of the suspension was approximately constant at any concentration of bacteria tested (0.9 – 1.8×10^{10} cells ml^{-1} ; figure 4b). For $S > 3 \text{ s}^{-1}$ the viscosity was found to decrease at increasing shear rates (shear thinning) at all cell concentrations (figure 4b), in line with what reported previously for *E. coli* suspensions [20]. Instead, a dense suspension of non-motile bacteria (figure 4a; black line) displayed a viscosity that monotonically decreased for increasing shear rates, the signature of a marked shear-thinning effect. As the predicted viscosity for a dispersion of

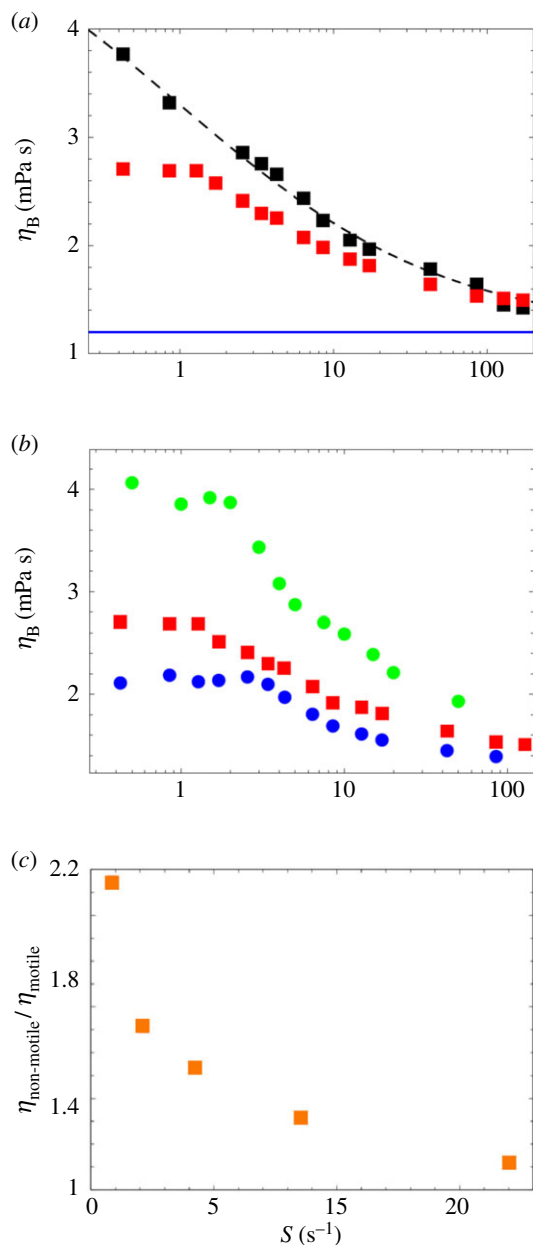


Figure 4. (a) Viscosity of a dense suspension of *Bacillus subtilis*, for motile (red squares) and non-motile (black squares) bacteria, measured using the microfluidic set-up described in [20], as a function of the mean absolute shear rate computed at mid-plane over the width of the channel, S . The cell concentration was 1.2×10^{10} cells ml^{-1} . The black dashed line represents the numerical fit of the experimental data used to implement the numerical simulations, $\eta = \eta_{\infty} + ((\eta_0 - \eta_{\infty}) / (1 + (S/S_0)^{0.57}))$, where $\eta_{\infty} = 1.2$ mPa s, $\eta_0 = 4.8$ mPa s and $S_0 = 1.9$ s^{-1} [25]. The blue full line represents the predicted value (μ_{∞}) for the viscosity of a dispersion of rigid rods having a similar aspect ratio and concentration to the bacterial suspensions used in our experiments according to [26]. (b) Viscosity of a dense suspension of motile *B. subtilis* bacteria as a function of shear rate S , for suspensions with different cell concentrations: 1.8×10^{10} cells ml^{-1} (green circles), 1.2×10^{10} cells ml^{-1} (red squares) and 0.9×10^{10} cells ml^{-1} (blue circles). (c) Ratio of the viscosity of a non-motile and a motile suspension of *B. subtilis* bacteria measured as a function of the mean shear rate S . The cell concentration was 1.7×10^{10} cells ml^{-1} .

rigid rods of similar aspect ratio and volume fraction (figure 4a, blue line) is expected to be Newtonian [23,25,26], the observed shear-thinning behaviour could be due to the extended network of limp bacterial flagella; however, in the limit of high shear, the viscosity of the bacterial suspension approaches the expected value of $\eta_{\infty} = 1.2$ mPa s (figure 4a). Remarkably,

η_{eff} was more than 30% lower for motile compared with non-motile suspensions at the lowest shear rate tested ($S \approx 0.4$ s^{-1}), whereas it was comparable for motile and non-motile suspensions at higher-shear rates ($S > 10$ s^{-1}) (figure 4c), in line with the convergence of the velocity profiles of the two suspensions towards a parabolic shape with increasing flow rate (figure 3b,c).

We used the dependence of the viscosity on the shear rate obtained from the microrheological measurements as input to a finite-element numerical model of the velocity profile for a suspension of non-motile bacteria. The model yielded velocity profiles in good agreement with the experimentally determined profiles, particularly for the higher flow rates (figure 3b,c, dashed lines). These observations are consistent with the plug-flow profiles observed with non-motile bacteria (figure 1c), because the lower viscosity in the higher-shear portion of the channel near the sidewalls increases the local flow velocity compared with a parabolic profile, whereas the higher viscosity in the lower-shear portion of the channel near the centreline decreases the local flow velocity.

The velocity variations in the flowing bacterial suspension were caused by active intermittency, not by the passive alternation of volumes of motile and non-motile bacteria rigidly transported by the imposed flow. This was found by following classic turbulence theory [27] and decomposing the velocity field, $U_x(x, y, t) = V_x(x, y) + u_x(x, y, t)$, into a time-averaged component, $V_x(x, y) = \langle U_x(x, y, t) \rangle_t$, where $\langle \dots \rangle_t$ denotes temporal averaging and $u_x(x, y, t)$ a fluctuating component (a similar equation applies to U_y). From the fluctuating velocities in the plane of observation, u_x and u_y , we computed the instantaneous turbulence intensity, $I(t) = (u_x^2 + u_y^2)^{1/2}$, of individual, small ($28 \mu\text{m}^2$) fluid elements of the bacterial suspension as a function of time, following each fluid element (figure 5a; we neglected u_z because $u_z^2 < u_x^2, u_y^2$ at channel mid-depth [28]). While fluid elements largely followed the mean flow, with only small cross-stream oscillations (figure 5a), the turbulence intensity of each element changed markedly over the course of its journey (figure 5b,c), with $I(t)$ varying between 0 and $45 \mu\text{m s}^{-1}$ over only a few seconds and sometimes exhibiting large, nearly periodic oscillations (figure 5b, pink). This analysis confirms that the entire bacterial suspension was always active during the course of the experiment and thus the intermittency did not result from a local quenching of bacterial motility.

We propose that the observed intermittency results from the presence of flow structures characteristic of bacterial turbulence, like vortices, interacting with the imposed flow. To test this hypothesis, we applied the λ -2 criterion, traditionally used in unsteady, wall-bounded turbulent flows to identify and track individual vortical structures as they are advected by the flow [21]. This criterion is particularly efficient in the identification of vortices in the presence of a background shear, a situation where other methods typically fail to distinguish between vortical structures and the vorticity generated in the shear layer. We found that an increase in the local streamwise velocity is generally associated with stronger vortices (i.e. vortex cores associated with high vorticity magnitude), located in the highest-shear regions near the channel sidewalls (figure 6a–d, black circles). The direction of rotation of these vortices is imparted by the vorticity of the imposed flow (as shown by the vorticity colour map in figure 6a–d) and results in vortices locally enhancing the streamwise velocity U_x near the centre of the channel (figure 6e–h). When vortices

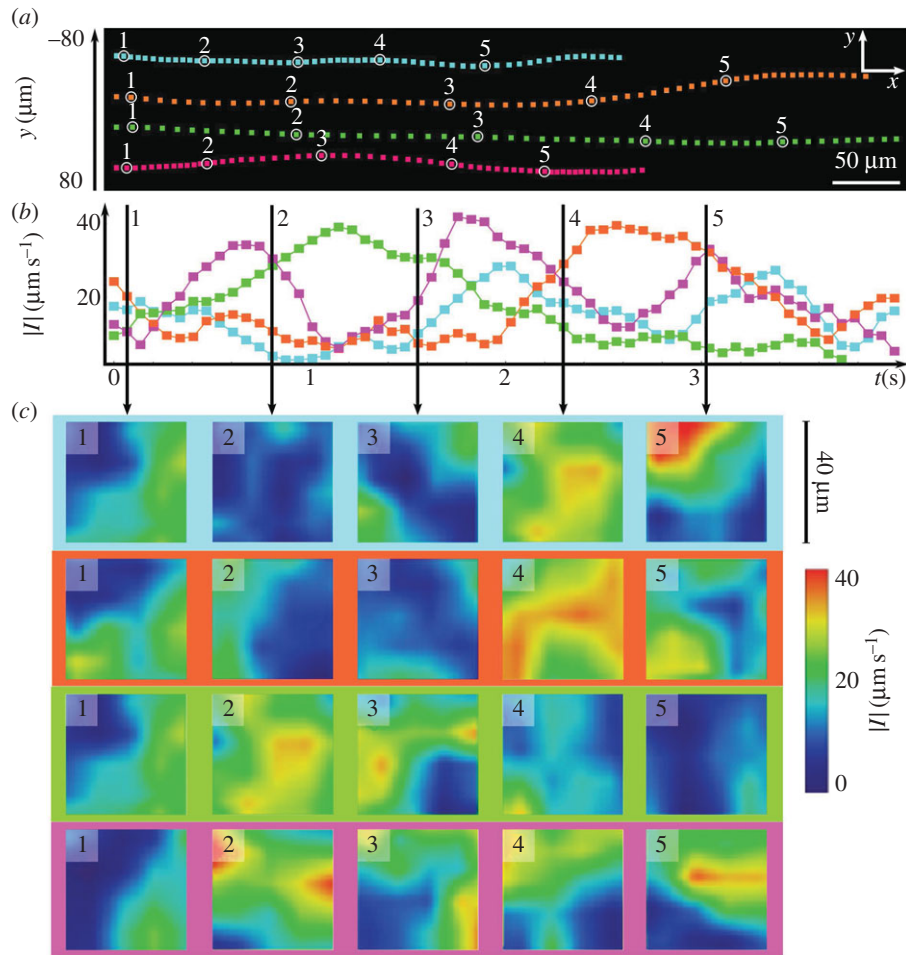


Figure 5. (a) Trajectories of four small ($28 \mu\text{m}^2$) fluid elements of the bacterial suspension. (b) Time series of the turbulence intensity, I , of each of the four blobs tracked in (a). (c) Local map of the turbulence intensity, I , within each blob, at the five times indicated in (b) and at the locations indicated in (a).

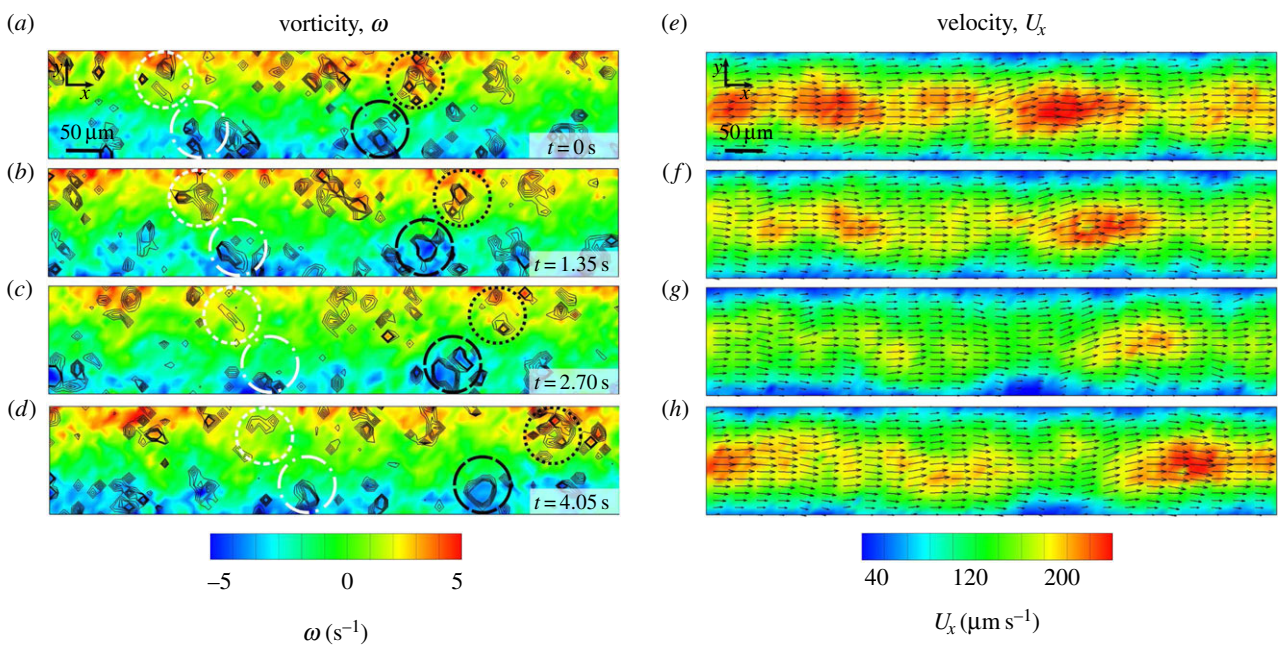


Figure 6. (a–d) Contour plots (solid lines) identify the core of vortices created by the collective motion of bacteria, obtained from the λ -2 analysis [21], where the direction of rotation is shown by the overlaid vorticity field (colour map). Dashed circles highlight the evolution of four representative vortices in the flowing suspension. Black circles indicate two vortices whose magnitude is sustained along the direction of the flow, while white circles highlight two decaying vortices. (e–h) Contour plots of the streamwise velocity U_x with velocity vectors.

decay in intensity (figure 6, white circles), the streamwise velocity also decreases in magnitude (figure 6e–h). This analysis therefore reveals how vortices spontaneously generated by the collective motion of bacteria can be either sustained or

dissipated by the mean flow and this in turn affects the mean velocity of the flowing suspension.

We further explored the connection between intermittency and coherent structures in the collective motion of

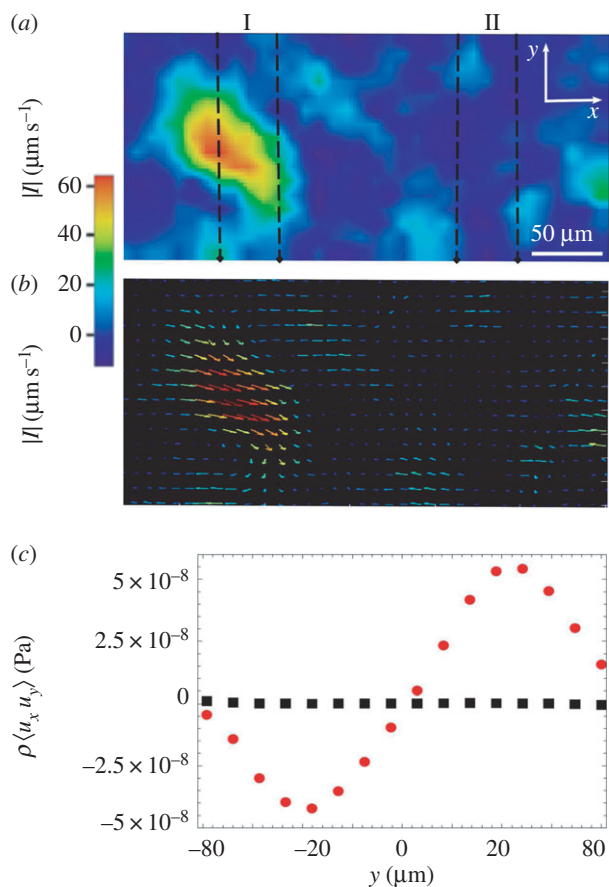


Figure 7. Map of the magnitude (a) and direction (b) of the turbulence intensity I , highlighting the strong difference between sections I and II (figure 1a). (c) Cross-channel profiles of the Reynolds stress for suspensions of motile bacteria (red circles) and non-motile bacteria (black squares) computed by averaging in time over the entire duration of the measurement (77 s) and along the streamwise dimension (x) of the observation window (840 μm in length).

bacteria by comparing the turbulence intensity field (figure 7a,b) with the streamwise velocity of the flowing suspension (figure 1a–c). This comparison shows that when the streamwise velocity profile U_x is parabolic (section I in figure 1a,b), the turbulence intensity I is higher and the velocity fluctuations correlate in the form of a vortex (section I in figure 7a,b). Conversely, when U_x has a plug-like profile (section II in figure 1a,b), I is considerably lower and the velocity fluctuations are largely uncorrelated. We therefore conclude that vortices interact with the externally imposed flow and cause it to change from the plug-flow default characteristic of non-motile bacteria (figure 1c) to the parabolic profile intermittently observed for motile bacteria (figure 1b).

In addition to providing a reference system for the presence of intermittency, classic turbulence theory supplies a statistical approach—the calculation of Reynolds stresses [27], which account for the strong enhancement in the transport of transverse momentum in classic turbulence—that can be adopted to explain the rheological properties of bacterial suspensions and is applicable here due to the presence of an imposed flow (Reynolds stresses vanish by symmetry in the absence of flow [27]). The effect of small-scale velocity fluctuations produced by the collective bacterial motion on the mean flow is characterized by a stress tensor $\sigma_{ij} = \eta \partial V_i / \partial x_j + \tau_{ij}$, where η and ρ are the fluid's dynamic viscosity and density, respectively, and $\tau_{ij} = -\rho \langle u_i u_j \rangle_t$ is the Reynolds

stress tensor [27], here obtained from the direct measurements of velocity fluctuations (figure 7c). In classic turbulence, $\eta \partial V_i / \partial x_j$ and τ_{ij} have the same sign [27]: small-scale motions dissipate energy coming from the large-scale flow. By contrast, in bacterial turbulence these two terms have opposite signs over the entire width of the channel, signifying that the energy expended by the bacteria 'pushes' the fluid and injects energy into the flowing suspension. The vanishing of the Reynolds stress in flowing suspensions of non-motile bacteria (figure 7c) proves that its origin lies in the combined action of external flow and active bacterial motion.

The occurrence of bacteria in the human gut microbiome in densities comparable to those used here [4] suggests that the ability to directly observe such dense suspensions under controlled conditions may provide a useful model system for certain microbiome dynamics. This view is reinforced by the fact that the gut microbiome habitat is characterized by shear rates (0.2–8 s^{-1} ; [24]) of the same order as those used in these experiments (2.2–13.5 s^{-1}). Clearly, however, there are also fundamental differences, including the presence of mucus, differences in chemical conditions, with oxygen scarcity and oxygen gradients probably being prevalent in the gut [29], as well as topographic complexity [30], vis-à-vis the simple rectangular shape of the microchannels used here. Finally, it remains unclear how prevalent motility is in the human gut microbiome [31]. Some of these environmental features could be captured relatively simply in future versions of microfluidic model systems, with the advantage of providing an imaging-based, biophysically focused approach that is complementary to and often lacking in the majority of molecularly based microbiome studies. Only through integration with physiological and molecular approaches, though, can the full implications of physical processes such as the intermittency observed here be realized.

4. Conclusion

The presented results demonstrate that the coupling between the collective motion of bacteria and an imposed flow triggers a distinctive intermittency in the flow of dense bacterial suspensions. This phenomenon bears a strong similarity with the intermittency observed at the onset of classic turbulence in pipe flow. In line with this similarity, the observed intermittency was characterized by the absence of any spatial or temporal regularity and disappeared at increasing flow rates. We demonstrated that this intermittency is associated with the motility of the bacteria and in particular with the transient occurrence of vortices in their collective motion. By demonstrating the rich dynamics of an active suspension in flow, this work sheds new light on how patterns and self-organization emerge out of a multiplicity of simple interactions driven by environmental cues, a paradigm of many different processes in natural systems, from the swarming of microorganisms [32] and fish schools [33] to pedestrian crowds [34]. Furthermore, these experiments highlight the potential of the microfluidic approach to mimic fundamental features of the complex environment of the human microbiome, including the density of bacterial populations and the presence of fluid flow, shear and surfaces.

Authors' contributions. E.S., R.R., S.B., R.P. and R.S. designed the study and analysed the data. E.S. and S.S. carried out experiments.

M.M.S. performed numerical simulations and analysed the dynamics of vortices. All authors participated in writing the manuscript and gave final approval for publication.

Competing interests. We declare we have no competing interests.

Funding. R.S. acknowledges support through NSF grants CBET-1066566 and CBET-0966000, and a Gordon and Betty Moore Marine Microbial

Initiative Investigator Award (GBMF3783). M.M.S. acknowledges funding provided by NSERC (Natural Sciences and Engineering Research Council of Canada). This research was partly supported by a Roberto Rocca grant from the MIT–Italy programme (to R.P. and R.S.).

Acknowledgements. We thank L. Bocquet, F. Menolascina and H. Stark for discussions.

References

- Penders J, Stobbering EE, Savelkoul PHM, Wolffs PFG. 2013 The human microbiome as a reservoir of antimicrobial resistance. *Front. Microbiol.* **4**, 87. (doi:10.3389/fmicb.2013.00087)
- Smith DC, Steward GF, Long RA, Azam F. 1995 Bacterial mediation of carbon fluxes during a diatom bloom in a mesocosm. *Deep Sea Res. Part II* **42**, 75–97. (doi:10.1016/0967-0645(95)00005-B)
- Ranjard L, Richaume A. 2001 Quantitative and qualitative microscale distribution of bacteria in soil. *Res. Microbiol.* **152**, 707–716. (doi:10.1016/S0923-2508(01)01251-7)
- Bures J *et al.* 2010 Small intestinal bacterial overgrowth syndrome. *World J. Gastroenterol.* **16**, 2978–2990. (doi:10.1007/s11938-001-0042-2)
- Cisneros LH, Cortez R, Dombrowski C, Goldstein RE, Kessler JO. 2007 Fluid dynamics of self-propelled microorganisms, from individuals to concentrated populations. *Exp. Fluids* **43**, 737–753. (doi:10.1007/s00348-007-0387-y)
- Sokolov A, Aranson IS, Kessler JO, Goldstein RE. 2007 Concentration dependence of the collective dynamics of swimming bacteria. *Phys. Rev. Lett.* **98**, 158102. (doi:10.1103/PhysRevLett.98.158102)
- Sokolov A, Aranson IS. 2012 Physical properties of collective motion in suspensions of bacteria. *Phys. Rev. Lett.* **109**, 248109. (doi:10.1103/PhysRevLett.109.248109)
- Dunkel J *et al.* 2013 Fluid dynamics of bacterial turbulence. *Phys. Rev. Lett.* **110**, 228102. (doi:10.1103/PhysRevLett.110.228102)
- Hatwalne Y, Ramaswamy S, Rao M, Simha RA. 2004 Rheology of active-particle suspensions. *Phys. Rev. Lett.* **92**, 118101. (doi:10.1103/PhysRevLett.92.118101)
- Marchetti MC *et al.* 2013 Hydrodynamics of soft active matter. *Rev. Mod. Phys.* **85**, 1143–1189. (doi:10.1103/RevModPhys.85.1143)
- Sumpter DJT. 2006 The principles of collective animal behavior. *Phil. Trans. R. Soc. B* **261**, 5–22. (doi:10.1098/rstb.2005.1733)
- Parrish JK, Viscido SV, Grünbaum D. 2002 Self-organized fish schools: an examination of emergent properties. *Biol. Bull.* **202**, 296–395. (doi:10.2307/1543482)
- Cavagna A *et al.* 2009 Scale-free correlations in starling flocks. *Proc. Natl Acad. Sci. USA* **107**, 11 865–11 870. (doi:10.1073/pnas.1005766107)
- Eckhardt B, Schneider TM, Hof B, Westerweel J. 2007 Turbulence transition in pipe flow. *Annu. Rev. Fluid Mech.* **39**, 447–468. (doi:10.1146/annurev.fluid.39.050905.110308)
- theLabRat.com. *Terrific Broth media recipe*. <http://www.thelabrat.com/protocols/TerrificBroth.shtml>
- McDonald JC *et al.* 2000 Fabrication of microfluidic systems in poly(dimethylsiloxane). *Electrophoresis* **21**, 27–40. (doi:10.1002/(SICI)1522-2683(20001011)21:1<27::AID-ELPS27>3.0.CO;2-C)
- Shiku H *et al.* 2006 Oxygen permeability of surface-modified poly(dimethylsiloxane) characterized by scanning electrochemical microscopy. *Chem. Lett.* **35**, 234–235. (doi:10.1246/cl.2006.234)
- Buzzaccaro S, Secchi E, Piazza R. 2013 Ghost particle velocimetry: accurate 3D flow visualization using standard lab equipment. *Phys. Rev. Lett.* **111**, 048101. (doi:10.1103/PhysRevLett.111.048101)
- Stanislas M *et al.* 2008 Main results of the third international PIV Challenge. *Exp. Fluids* **45**, 27–71. (doi:10.1007/s00348-008-0462-z)
- Gachelin J *et al.* 2013 Non-Newtonian viscosity of *Escherichia coli* suspensions. *Phys. Rev. Lett.* **110**, 268103. (doi:10.1103/PhysRevLett.110.268103)
- Jeong J, Hussain F. 1995 On the identification of a vortex. *J. Fluid Mech.* **285**, 69–94. (doi:10.1017/S0022112095000462)
- Tang HS, Kalyon DM. 2004 Estimation of the parameters of Herschel–Bulkley fluid under wall slip using a combination of capillary and squeeze flow viscometers. *Rheol. Acta* **43**, 80–88. (doi:10.1007/s00397-003-0322-y)
- Wierenga AM, Philipps AP. 1998 Low-shear viscosity of isotropic dispersions of (Brownian) rods and fibres; a review of theory and experiments. *Colloids Surf. A* **137**, 355–372. (doi:10.1016/S0927-7757(97)00262-8)
- Kim HJ, Huh D, Hamilton G, Ingber DE. 2012 Human gut-on-a-chip inhabited by microbial flora that experiences intestinal peristalsis-like motions and flow. *Lab. Chip* **12**, 2165–2174. (doi:10.1039/c2lc40074j)
- Spagnolie S. 2015 *Complex fluids in biological systems: experiment, theory, and computation*. Berlin, Germany: Springer.
- Ortega A, Garcia de la Torre J. 2003 Hydrodynamic properties of rodlike and disklike particles in dilute solution. *J. Chem. Phys.* **119**, 9914–9919. (doi:10.1063/1.1615967)
- Tennekes H, Lumley JL. 1972 *A first course in turbulence*. Cambridge, MA: MIT Press.
- Rusconi R, Guasto JS, Stocker R. 2014 Bacterial transport suppressed by fluid shear. *Nat. Phys.* **10**, 212–217. (doi:10.1038/nphys2883)
- Albenberg L *et al.* 2014 Correlation between intraluminal oxygen gradient and radial partitioning of intestinal microbiota. *Gastroenterology* **47**, 1055–1063. (doi:10.1053/j.gastro.2014.07.020)
- Nguyen TLA, Vieira-Silva S, Liston A, Raes J. 2015 How informative is the mouse for human gut microbiota research? *Dis. Models Mech.* **8**, 1–16. (doi:10.1242/dmm.017400)
- Cullender TC *et al.* 2013 Innate and adaptive immunity interact to quench microbiome flagellar motility in the gut. *Cell Host Microbe* **14**, 571–581. (doi:10.1016/j.chom.2013.10.009)
- Zhang HP *et al.* 2009 Swarming dynamics in bacterial colonies. *Europhys. Lett.* **87**, 48011. (doi:10.1209/0295-5075/87/48011)
- Flierl G, Grunbaum D, Levin S, Olson D. 1999 From individuals to aggregations: the interplay between behavior and physics. *J. Theor. Biol.* **196**, 397–454. (doi:10.1006/jtbi.1998.0842)
- Helbing D *et al.* 2005 Self-organized pedestrian crowd dynamics: experiments, simulations, and design solutions. *Transp. Sci.* **39**, 1–24. (doi:10.1287/trsc.1040.0108)